DOI:10.25092/baunfbed.826433 *J. BAUN Inst. Sci. Technol., 23(1), 50-64, (2021)*

The structural and optical properties of Al and Mg doped ZnO synthesized by solid state reaction method

Özlem BİLGİLİ*

Dokuz Eylül University, Faculty of Science, Department of Physics, Tınaztepe Campus, İzmir

Geliş Tarihi (Received Date): 09.01.2020
Kabul Tarihi (Accepted Date): 09.06.2020

Abstract

In this study, the structural and optical properties of Al and Mg doped zinc oxide $Zn_{0.98}M_{0.02}O$ (M= Al, Mg) prepared by solid state reaction method is investigated. X-ray diffraction (XRD), Scanning Electron Microscopy (SEM), UV-Visible spectroscopy (UV–Vis) and Fourier Transform Infrared (FTIR) spectroscopy were employed to study the structural and optical properties. With XRD analysis, it was revealed that all the samples are hexagonal wurtzite structure and exhibit no impurity phases. The reflectance spectra was used to determine the optical band gap of the samples. And it was found that undoped ZnO sample has an energy band gap of 3.16 eV which increases with Al and Mg doping, probably driven by the decrease in the lattice parameters. The structural bond vibrations of undoped and doped ZnO were analysed by FTIR spectroscopy, and it was seen that the broad absorption band is at approximately 550 cm^{-1} for all the samples, which corresponds to the stretching vibration of Zn–O bond.

***Keywords**: Semiconductors, ZnO, XRD, UV-Visible spectroscopy, FTIR, SEM.*

* Özlem BİLGİLİ, ozlem.bilgili@deu.edu.tr, http://orcid.org/0000-0002-6334-2513

Katıhal reaksiyon yöntemi ile sentezlenen Al ve Mg katkılı ZnO' nun yapısal ve optik özellikleri

Öz

Bu çalışmada, katıhal reaksiyon yöntemi ile hazırlanan Al ve Mg katkılı çinko oksidin $Zn_{0.98}M_{0.02}O$ (M = Al, Mg) yapısal ve optik özellikleri incelenmiştir. Yapısal ve optik özellikleri incelemek için X-ışını kırınımı (XRD), Taramalı Elektron Mikroskobu (SEM), UV-Görünür spektroskopisi (UV-Vis) ve Fourier Dönüşümü Kızılötesi (FTIR) spektroskopisi kullanılmıştır. XRD analizi ile tüm örneklerin altıgen wurtzite yapıda olduğu ve hiçbir safsızlık fazı olmadığı ortaya çıkmıştır. Yansıma spektrumları örneklerin optik bant aralığını belirlemek için kullanılmıştır. Katkısız ZnO örneğinin 3.16 eV enerji band aralığına sahip olduğu ve Al ve Mg katkısı ile arttığı gözlenmiştir, ki bu muhtemelen örgü parametrelerindeki düşüşten kaynaklanmaktadır. Katkısız ve katkılı ZnO' nun yapısal bağ titreşimleri FTIR spektroskopisi ile analiz edilmiştir, ve tüm örnekler için Zn-O bağının, gerilme titreşimine karşılık gelen, geniş soğrulma bandının yaklaşık 550 cm^{-1}' de olduğu görülmüştür.

Anahtar kelimeler: *Yarıiletkenler, ZnO, XRD, UV-Görünür spektroskopisi, FTIR, SEM.*

1. Introduction

Zinc oxide (ZnO) is an II-VI semiconductor having a wide direct band gap energy (3.37 eV) at room temperature and a large exciton binding energy (60 meV). Due to its features, ZnO is suitable for short-wavelength optoelectronic applications. Further, because of its properties like low cost, non-toxicity, abundance in nature, and suitability to doping, ZnO has wide device applications in different areas, such as ultraviolet light-emitters, gas sensors, piezoelectric transducers and solar cells [1-7].

Many studies have been deployed to optimize the optical and structural properties of ZnO materials, properties of ZnO, particularly a major challenge is incorporation of doping ions into the ZnO lattice. Doping with proper elements, such as Al, Mn, Cd, Mg, Ni, and Cr, is an effective method to improve and control the structural and optical properties of ZnO nanoparticles. Additionally, doping with Group II elements (Cd, Mg) may change the value of the band gap and increase the intensity of UV emission [14-18]. ZnO has high electrical resistivity, which is a disadvantage and can be reduced by adding group III ions (B^{3+}, Al^{3+}, Ga^{3+}, and In^{3+}). These ions improve ZnO optical and electrical properties providing extra electrons. Al^{3+} is the element mostly selected as dopant due to its small ionic radius and low material cost. The substitution of Zn^{2+} ions with Al^{3+} in ZnO lattice causes electrical conductivity to increase with the increase of charge carriers [19-22].

The purpose of this study is to investigate the effects of Al and Mg doping on the structural and optical properties of ZnO prepared by the solid state reaction method. The effects of doping on structural and morphological properties were analyzed by X-ray diffractometer (XRD), Fourier transform infrared spectroscopy (FTIR), Scanning electron microscope (SEM) and the optical absorption studies were performed by UV–Visible spectroscopy.

2. Material and method

Samples of nominal compositions $Zn_{0.98}M_{0.02}O$ (M= Al, Mg) were synthesized via solid state reaction method. The stoichiometric amounts of starting powders ZnO, Al_2O_3 and MgO were mixed and ground followed by calcination at 400 ^oC for 8 h. After cooling, the resulting material was reground and pelletized. Finally, pellets of 10 mm diameter were prepared using press and sintered at 500 ^oC for 12 h.

The crystalline structure of the samples was characterized by using XRD in 2θ range of 20-80 degrees. The phase and crystal parameters of all samples were determined using CuK_α radiation (λ= 1.5406 Å). The major diffraction peaks for all the samples can be indexed to the hexagonal wurtzite structure of ZnO crystal with reference to Joint Committee on Powder Diffraction Standards (JCPDS) file No. 36-1451. The optical properties of the samples were characterized by using ultraviolet-visible spectrometer (UV–Vis). UV–Vis reflectance spectra of the samples were recorded in the wavelength range of 300 to 800 nm. The band gap of undoped and doped ZnO was identified by UV–Vis reflectance spectra recorded. The bonding between different atoms and chemical properties of the particles was analysed by FTIR spectra. The FTIR spectrum was gathered between the wavenumber of 400 and 4000 cm^{-1}. The surface morphology and grain size of the samples were studied by employing SEM.

3. Results

XRD patterns of the undoped, Al doped and Mg doped ZnO samples are illustrated in Figure 1. XRD peaks at angle 2θ are 31.8°, 34.5°, 36.3°, 47.6°, 56.6°, 62.9°, 66.4°, 68.0°, 70.0°, 72.6° and 77.0° which are indexed as miller indices (100), (002), (101), (102), (110), (103), (200), (112), (201), (004) and (202) corresponding to ZnO, respectively (space group p63mc, JCPDS no.36–1451) indicating that the phase of the samples are hexagonal wurtzite structure. As seen from XRD patterns, there are no secondary phases with Mg and Al doping into ZnO crystal lattice and notable changes are not detected in the XRD patterns.

XRD analysis enables studying the effects of Al and Mg ions on the crystallite size and lattice parameters. The lattice parameters were calculated from the relationship of the interplanar spacing of the {hkl} plane for the wurtzite structure and the lattice parameters by the Miller indices hkl using the below relationship [23]:

$$a = \frac{\lambda}{\sqrt{3}sin\theta}\sqrt{h^2 + hk + k^2} \quad (1)$$

$$c = \frac{\lambda}{2sin\theta} \quad (2)$$

The following equation is used to calculate the volume of the unit cell for hexagonal system [24]:

$$V = \frac{\sqrt{3}a^2c}{2} = 0.866a^2c \quad (3)$$

The obtained values are listed in Table 1. The lattice parameters for undoped ZnO were found to be a= 3.2502±0.0001 Å, c= 5.2027±0.0005 Å and the volume is 47.60±0.0001 $Å^3$. The calculated lattice constants are in line with 36-1451 JCPDS standard data (a= 3.2498 Å and c= 5.2066 Å). The lattice parameters calculated from XRD data of $Zn_{0.98}Al_{0.02}O$ powder are a= 3.2484 ± 0.0008 Å, c= 5.2008±0.0020 Å, and the volume is 47.53±0.0003 $Å^3$ and $Zn_{0.98}Mg_{0.02}O$ powder are a= 3.2479± 0.0008 Å and c= 5.1966±0.0023 Å, and the volume is 47.47±0.0002 $Å^3$. The lattice parameters decrease slightly with Al and Mg doping. Al^{3+} has a smaller ionic radius (0.54 Å) than that of Zn^{2+} (0.74 Å), and the substitution of Al into ZnO may be the reason for the decrease in the lattice parameter. Mg^{2+} ionic radius (0.72 Å) is comparable to the Zn^{2+} ionic radius (0.74 Å), thus the decrease may be due to the electronegativity difference between Zn and Mg, inducing an effect of the interaction of Mg^{2+} ions with O^{2-} ions. This leads to a compression of the structure along the c axis [25, 26].

The c/a ratio is 1.633 in a stoichiometric wurtzite structure [27]. The c/a ratio of undoped, Al and Mg doped ZnO samples are 1.607, 1.601, 1.600, respectively. As seen, c/a ratio of all samples is significantly smaller than ideal which might be linked to the presence of oxygen vacancies V_O and extended defects.

Atomic packing fraction (APF) was determined by [28]:

$$APF = \frac{2\pi a}{(3\sqrt{3}\, c)} \tag{4}$$

where a and c are the lattice parameters. The value of APF for all samples, which decreases with doping indicating the increase of voids in the samples, is listed in Table 2. The APF of bulk hexagonal ZnO materials is about 74%, however in this study, the APF of $Zn_{0.98}M_{0.02}O$ nanoparticles is nearly 75% in hexagonal structure, this can be related to the substitutional effect of Al and Mg.

For hexagonal structure of ZnO, the Zn–O bond length L is calculated using the following relations. The bond length *L* for Zn–O is given by:

$$L = \sqrt{\frac{a^2}{3} + (\frac{1}{2} - u)^2 c^2} \tag{5}$$

where a, c are the lattice parameters and u is the positional parameter of the wurtzite structure. u is a measure of the amount by which atom is displaced with respect to the next along the c-axis. The parameter u in the wurtzite structure is given by [29,30]:

$$u = \left(\frac{a^2}{3c^2} + 0.25\right) \tag{6}$$

The calculated Zn-O bond length (L) values are summarized in Table 1. Bond lengths (L) were obtained as 1.9765 Å, 1.9758 Å and 1.9775 Å in Al, Mg doped and undoped ZnO samples, respectively. This trend is similar to the one in the lattice parameters and also agrees with Zn-O bond length in the unit cell. The ionic radius of O^{2-} is 1.21 Å, the ionic radius of the Zn^{2+} is 0.74 Å and thus, the length of the Zn-O bond is 1.95 Å. The calculated values in all samples are slightly higher than 1.95 Å. This result reveals that there are structural defects, especially oxygen vacancies [31]. The oxygen positional

parameter (u) calculated for undoped ZnO, Al and Mg doped samples are 0.38009, 0.38004 and 0.38021, respectively.

The lattice parameters, unit cell volume, and the Zn-O bond length change with Al and Mg doping, also depicted in Table 1. The crystal parameter value of doped samples, in general, is smaller than the value of undoped ZnO. This shows that Al^{3+} or Mg^{2+}, which both have an ionic radius smaller than Zn^{2+} ions, substitute into the ZnO lattice. When Al^{3+} or Mg^{2+} ions fill Zn^{2+} ion lattice, this causes crystal defects and charge imbalance in ZnO structure.

The average crystallite size (D) is determined using the Scherrer's formula (ignoring the effect of strain):

$$D = (K\lambda)/\beta_{hkl}cos\theta \tag{7}$$

where D is crystallite size in nanometer, β is the full width of diffraction peak at half of the maximum intensity (FWHM) in radians, K (= 0.9) is shape factor and λ (= 0.154 nm) is the wavelength of CuK_α radiation and θ is the peak position for corresponding hkl [32]. The calculated grain size of the samples is 38.12 nm, 36.00 and 39.14 nm for undoped, Al and Mg doped ZnO, respectively and listed in Table 2. Al^{3+} has a small ionic radius and thus easily penetrates into ZnO crystal lattice and in turn, decreases the average crystallite size. In contrast, Mg doping in ZnO results in an increase of the crystallite size.

The average crystallite size and lattice strain are calculated by the Williamson–Hall method. The two sources for the broadening of diffraction peaks, in this method, are crystallite sizes and inhomogeneous strain. The crystallite size and strain induced broadening are linked by the following relationship:

$$\beta_{hkl}cos\theta = \left(\frac{K\lambda}{D}\right) + (4\varepsilon sin\theta) \tag{8}$$

where β is the FWHM (rad), D is the crystallite size (nm), λ is the X-ray wavelength and ε is the strain induced on the particle [33-34]. Plots shown in Figure 2 are drawn with 4sinθ along the x-axis and βcosθ along the y-axis. Selected high intense peaks (100), (002), (101), (102), (110), (103) and (112) are used to determine the crystallite size and strain in all samples. The crystallite size and strain due to lattice deformation in the sample can be obtained from the inverse of the intercept at the y-axis and slope, respectively. The obtained results show a positive slope, and this indicates the tensile strain. The lattice strain and crystalline size of the samples are expected to have a significant effect on the optical properties [35].

The crystallite size for undoped, Al and Mg doped ZnO samples are calculated as 62.46, 56.82 and 64.49 nm, respectively, and the microstrain are calculated as 0.00118, 0.00118 and 0.00114 units for undoped, Al and Mg doped ZnO samples, respectively. The strain values calculated were found to decrease with Mg doping and increase with Al doping, this can be interpreted as the incorporation of dopants in the ZnO lattice. The decrease of strain may result in the increase of crystal size and reduction in the peak broadening, while the increase of strain may result in the reduction of crystal size and increase of peak broadening. The values are listed in Table 2. The crystallite size estimated using W–H plots followed the same trend as observed in Debye Scherrer's

formula. The particle size reported using Scherrer's Formula is smaller than the particle size observed. The difference in crystallite size estimated from Scherrer relation and that from WH plot calculation is mostly linked to the inclusion of strain in the samples and their estimated strain values are reasonable.

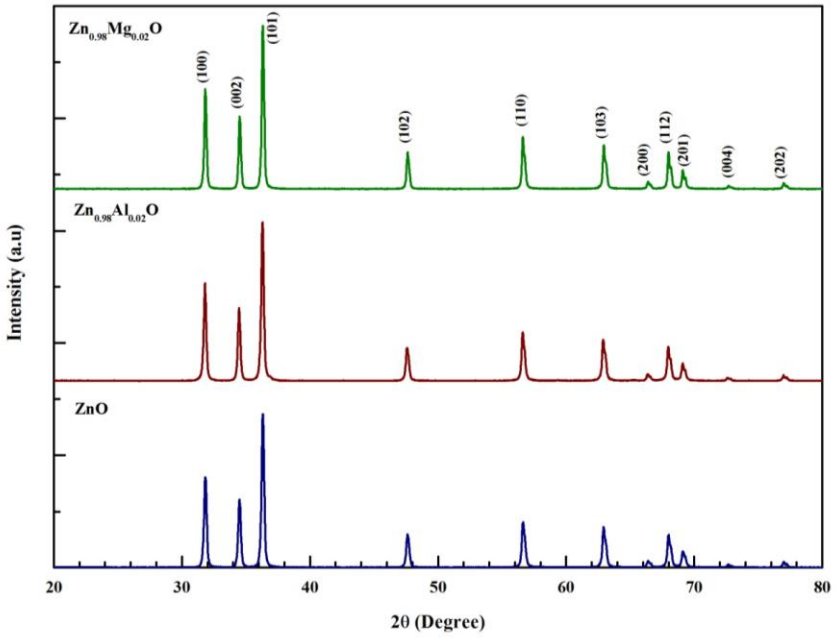

Figure 1. XRD patterns of undoped, Al and Mg doped ZnO samples.

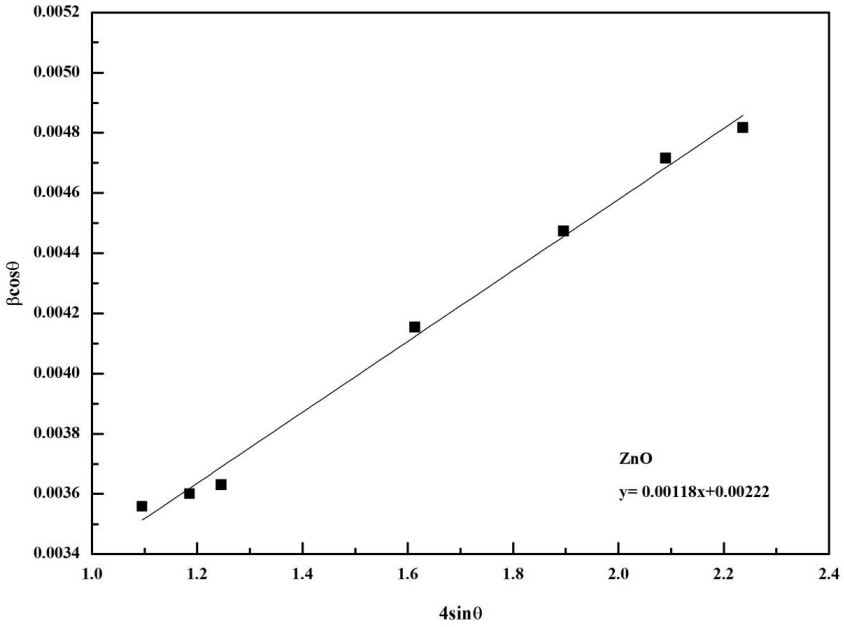

Figure 2. The Williamson-Hall analysis of (a) undoped, (b) Al and (c) Mg doped ZnO samples.

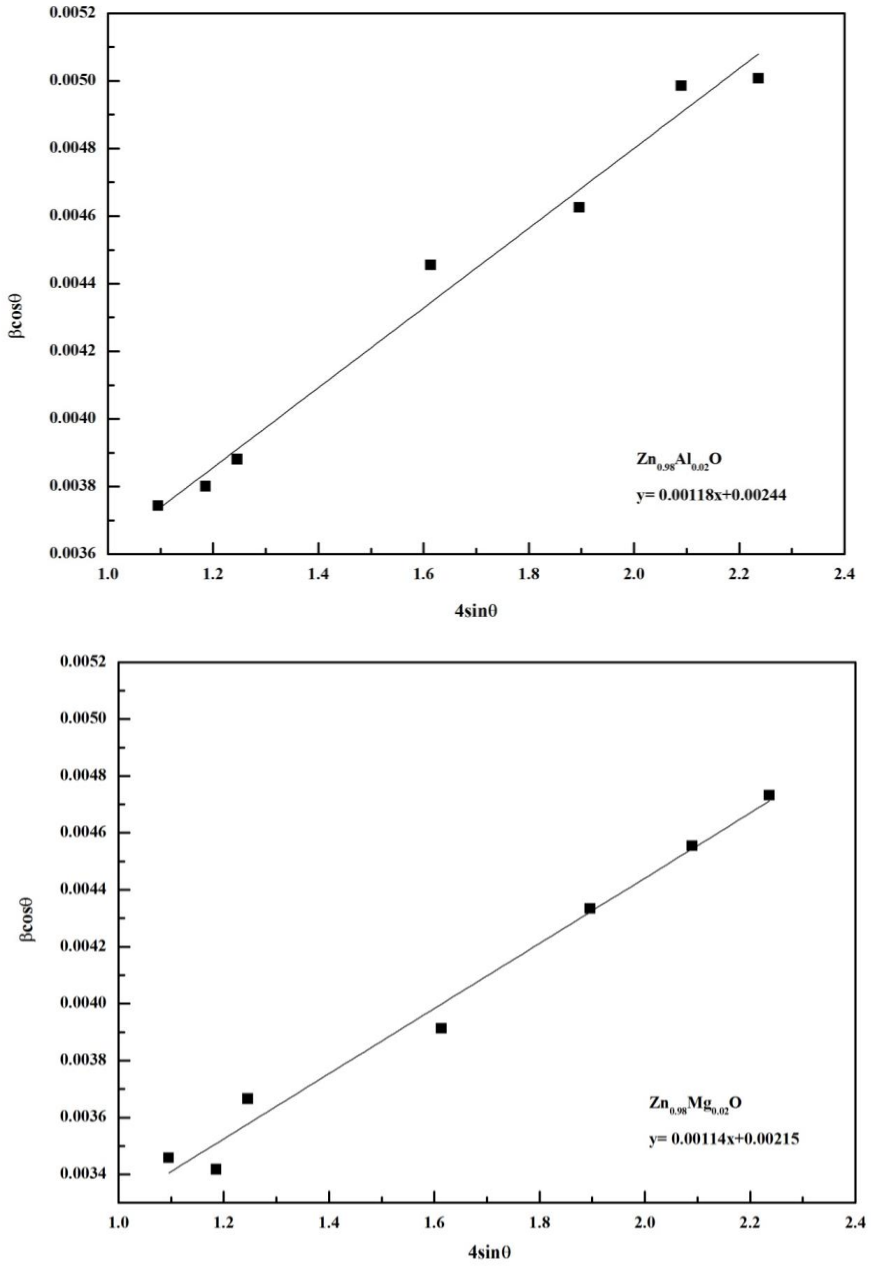

Figure 2. (Continued).

Table 1. Lattice parameters a and c, unit cell volume, lattice distortion c/a, positional parameter (u) and Zn-O bond length (L) of undoped ZnO and $Zn_{0.98}M_{0.02}O$ (M= Al, Mg).

Samples	**Lattice parameters (Å)**		**Volume of unit cell (Å³)**	**c/a**	**u**	**Zn-O bond Length (L) (Å)**
	a (Å)	**c (Å)**				
ZnO	3.2502(1)	5.2027(5)	47.60(1)	1.6007	0.38009	1.9775
$Zn_{0.98}Al_{0.02}O$	3.2484(8)	5.2008(20)	47.53(3)	1.6010	0.38004	1.9765
$Zn_{0.98}Mg_{0.02}O$	3.2479(8)	5.1966(23)	47.47(2)	1.6000	0.38021	1.9758

Table 2. Calculated size of the particles, microstrain values and APF of undoped ZnO and $Zn_{0.98}M_{0.02}O$ (M= Al, Mg).

Samples	**Crystallite size (nm) (Debye-Scherrer)**	**Crystallite size (nm) (W-H plot)**	**ε no unit**	**APF**
ZnO	38.12	62.46	0.00118	0.75502
$Zn_{0.98}Al_{0.02}O$	36.00	56.82	0.00118	0.75488
$Zn_{0.98}Mg_{0.02}O$	39.14	64.49	0.00114	0.75537

UV-Vis reflectance spectra of the samples as a function of the wavelength range from 300 to 800 nm are shown in Figure 3. The entrance of the dopants into ZnO lattice may be associated with the decrease observed in the amount of reflectance. And a further strong decrease that was seen in the reflectance spectra after 450 nm, is linked to the optical transitions occurring in the optical band gap.

The optical band gap Eg of ZnO values were determined by the conversion of the reflectance values to absorbance. The Kubelka–Munk equation is used to convert the reflectance spectra to the equivalent of absorption spectra [36, 37]:

$$F(R) = \frac{(1-R)^2}{2R} \quad (9)$$

F(R) and R are the equivalent of the absorption coefficient and the reflectivity, respectively.

The band gap energy of undoped and doped samples can be determined by using the Tauc relation [38-40]:

$$\alpha h\nu = B(h\nu - E_g)^n \quad (10)$$

where α is the absorption coefficient ($\alpha = F(R)/t$ and t is the thickness of the sample), hν is the incident photon energy (hν= 1240/wavelength), B is a constant which is related to the effective masses associated with the bands and E_g is the electronic energy of the optical band gap. The photon energy is determined by h, the Planck's constant (6.626×10^{-34} Js) and v, the frequency= c/λ, where c is the velocity of light (2.998×10^{8} m/s) and λ is the wavelength of light. The value of n = 1/2, 3/2, 2 or 3 depending on the nature of the electronic transition responsible for absorption, which is 1/2 for direct band gap material and 2 for indirect band gap material. ZnO has a direct band gap, thus in Equation, n = ½.

The curve of $(\alpha h\nu)^2$ vs. $h\nu$ for ZnO was plotted, as shown in Figure 4. The optical band gap Eg of all samples was determined from the intercept of the linear portion of the curve $(\alpha h\nu)^2$ to y = 0 and was found to be 3.16 eV, which is lower than the band gap of bulk ZnO materials (3.37 eV). This suggests that the optical band gap of ZnO semiconductor depends on the synthesis method used. The optical band gap increases from 3.16 eV to 3.25 and to 3.21 eV for Al and Mg doped ZnO, respectively. These results are listed in Table 3. The decrease in the crystallite size may be the cause of this increase in the optical band gap of the samples.

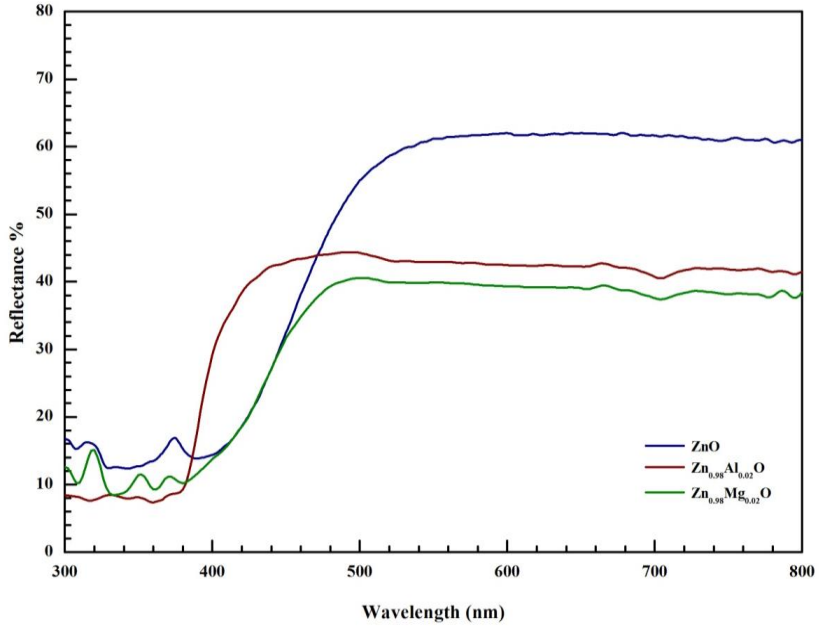

Figure 3. Reflectance spectra of undoped, Al and Mg doped ZnO samples.

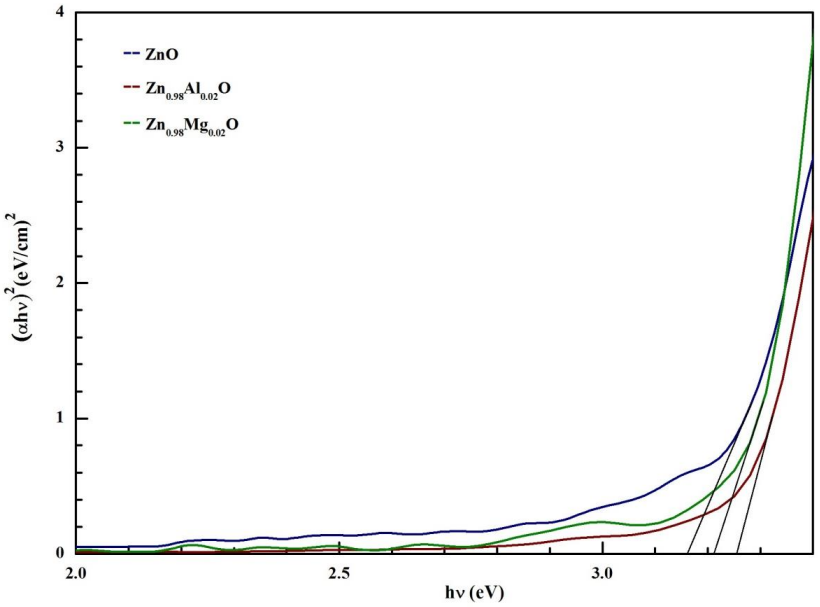

Figure 4. $(\alpha h\nu)^2$ versus hν for undoped, Al and Mg doped ZnO samples.

Table 3. Variation of optical band gap of undoped ZnO and $Zn_{0.98}M_{0.02}O$ (M= Al, Mg).

Samples	**Band gap (eV)**
ZnO	3.16
$Zn_{0.98}Al_{0.02}O$	3.25
$Zn_{0.98}Mg_{0.02}O$	3.21

The vibrational mode and chemical bonding of the samples were studied with FTIR spectroscopy. All measurements were recorded in the wavenumber range 4000 to 400 cm^{-1} and the results are shown in Figure 5. The strong vibrational mode which was observed in all samples at 500–550 cm^{-1}, can be attributed to Zn–O stretching in the

ZnO lattice. In Mg doped sample, the peak of the Zn–O band slightly shifts to a lower wavenumber, whereas in Al doped sample, it shifts slightly to a higher wavenumber. This shift may be associated with the change in the lattice parameters of ZnO. The absorption bands related to CO_2 absorbed from the atmosphere were detected between 2150 cm^{-1} and 1976 cm^{-1}. The band frequencies at around 2979, 2890 cm^{-1} belong to CH_2 stretching vibration. Such bands are not considered as contamination in samples. These vibrational bands present the existence of absorbed groups on the surface of nanocrystals and hence may be disregarded. The peaks observed in the region 3650-3750 cm^{-1} corresponds to O-H stretching vibrations which indicates the existence of water adsorbed on the surface of the samples [41-44]. Wide bands are at 703 cm^{-1} for Al doped sample, which attributes to the Al–O stretching vibration and does not exist in the undoped sample.

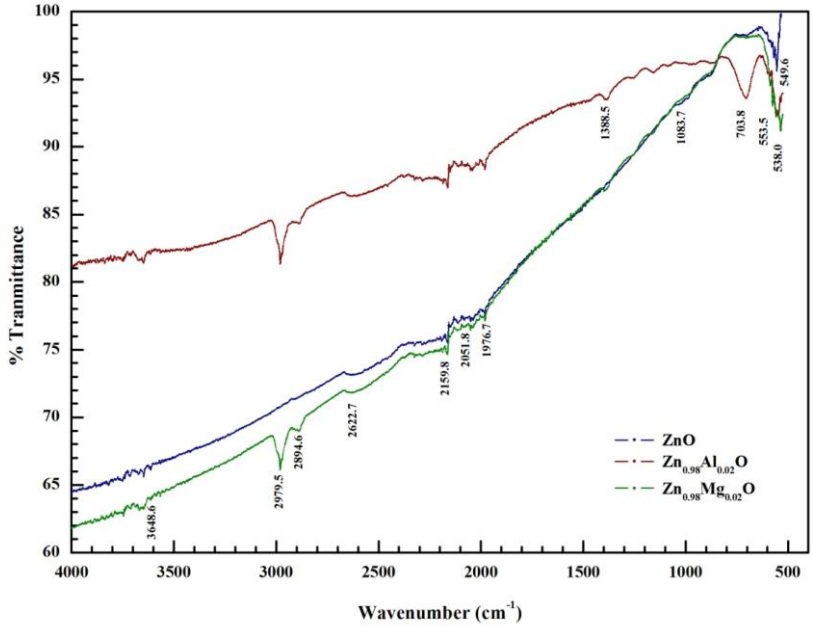

Figure 5. FTIR spectra of undoped ZnO and $Zn_{0.98}M_{0.02}O$ (M= Al, Mg).

The surface morphology for undoped ZnO, Al and Mg doped ZnO samples was investigated by SEM and displayed in Figure 6. The grains of the samples are homogeneously distributed and hexagonal like grains were observed in all samples. SEM images of the undoped sample reveal that grains are more closely packed and have larger sizes when compared to the doped samples. The pores/voids between the grains increase with doping, which may be attributed to the existence of defects due to substitution. It is seen from SEM images that the grain size becomes smaller with Al doping, and slightly larger with Mg doping when compared to the undoped sample. These results are in good agreement with the particle sizes obtained from XRD.

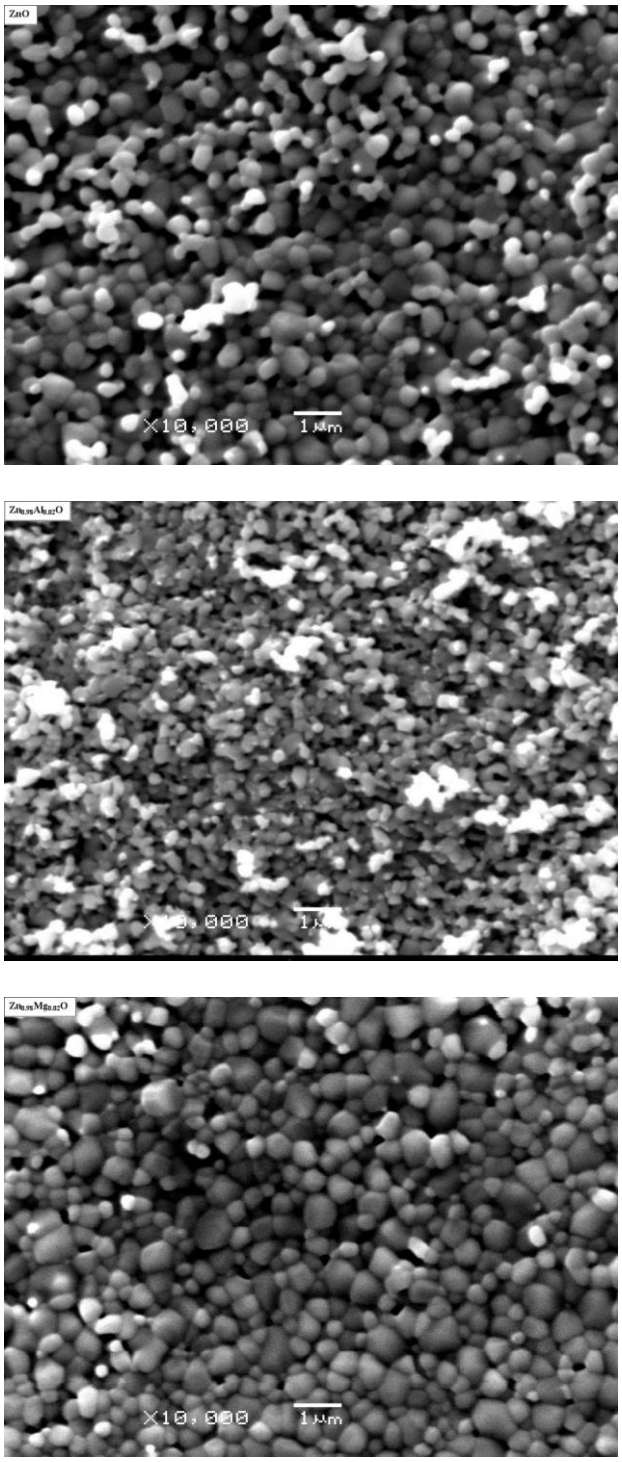

Figure 6. SEM images of (a) undoped, (b) Al and (c) Mg doped ZnO samples.

4. Discussion and conclusion

In this work, $Zn_{0.98}M_{0.02}O$ (M= Al, Mg) was synthesized by solid state reaction method. The effects of doping on the structural and optical properties of undoped and doped ZnO were studied by using XRD, UV–vis spectra, FTIR and SEM. All samples have a hexagonal wurtzite structure without any impurity phases, as revealed by XRD patterns. The reflectance decreases as a result of the incorporation of dopants into ZnO. The

optical band gaps of all samples were determined from reflectance measurements. The band gap is 3.16 eV for the undoped sample, and it increases to 3.25 and to 3.21 eV for Al and Mg doped samples, respectively. Zn–O band shifts slightly towards to a lower wavenumber with Mg doping and to a higher wavenumber with Al doping, as observed from FTIR analysis. SEM images reveal that all samples have grains mainly in hexagonal form. Also, it is shown that the grain size and grain distributions of the samples change depending on the dopant content. Overall, the experimental results conclude that the structural and optical characteristics such as crystal size, lattice parameters, band gap may be modified with doping in ZnO system.

References

[1] Abaira, R., Dammak, T., Matoussi, A., Younes, A., Structural and optical properties of zinc oxide doped by V_2O_5 synthesized by solid-state reaction, **Superlattices and Microstructures**, 91, 365-374, (2016).

[2] Koseoglu, Y., Durmaz, Y. C., Yilgin, R., Rapid synthesis and room temperature ferromagnetism of Ni doped ZnO DMS nanoflakes, **Ceramics International**, 40, 10685-10691, (2014).

[3] Akilan, T., Srinivasan, N., Saravanan, R., Magnetic and optical properties of Ti doped ZnO prepared by solid state reaction method, **Materials Science in Semiconductor Processing**, 30, 381-387, (2015).

[4] Jin, C., Yuan, X., Ge, W., Hong, J., Xin, X., Synthesis of ZnO nanorods by solid state reaction at room temperature, **Nanotechnology**, 14. 667-669, (2003).

[5] Das, T., Das, B. K., Parashar, K., Parashar, S. K., Temperature and frequency dependence electrical properties of Zn1-xCaxO nanoceramic, **Acta Physica Polonica A**, 130, 1358-1362, (2016).

[6] Elilarassi, R., Chandrasekaran, G., Structural, optical and magnetic characterization of Cu-doped ZnO nanoparticles synthesized using solid state reaction method, **Journal of Materials Science Materials in Electronics**, 21, 1168-1173, (2010).

[7] Lin, J. M., Zhang, Y. Z., Ye, Z. Z., Gu, X. Q., Pan, X. H., Yang, Y. F., Lu, J. G., He, H. P., Zhao, B. H., Nb-doped ZnO transparent conducting films fabricated by pulsed laser deposition, **Applied Surface Science**, 255, 6460–6463, (2009).

[8] Ahn, G. Y., Park, S., Kim, C. S., Enhanced ferromagnetic properties of diluted Fe doped ZnO with hydrogen treatment, **Journal of Magnetism and Magnetic Materials**, 303, 329-331, (2006).

[9] Ahmed, S. A., Effects of annealing temperature and dopant concentration on the structure, optical, and magnetic properties of Cu-doped ZnO nanopowders, **Journal of Materials Science Materials in Electronics**, 28, 3733-3739, (2017).

[10] Karamat, S., Ke, C., Tan, T. L., Zhou, W., Lee, P., Rawat, R. S., Investigation of impurity phase formation for (ZnO)1-x(TMO)x bulk samples formed by ball milling, **Applied Surface Science**, 255, 4814-4820, (2009).

[11] Nahm, C., Nb2O5 doping effect on electrical properties of ZnO–V2O5–Mn3O4 varistor ceramics, **Ceramics International**, 38. 5281–5285, (2012).

[12] Ahmed, S. A., Effects of Cu and Mn dopings on the structural, optical, and magnetic properties of Zn0.98Fe0.02O nanopowders, **Journal of Materials Science**, 52, 4977–4987, (2017).

[13] Modwi, A., Lemine, O. M., Alshammari, M., Houas, A., Ferromagnetism at room temperature in Zn0.95Cu0.05O nanoparticles synthesized by sol-gel method, **Materials Letters**, 194, 98–101, (2017).

[14] Shayesteh S. F., Dizgah, A. A., Effect of doping and annealing on the physical properties of ZnO:Mg nanoparticles, **Pramana journal of physics**, 81, 319–330, (2013).

[15] Hallani, G. E., Nasih, S., Fazouan, N., Liba, A., Khuili, M., Sajieddine, M., Mabrouki, M., Laanab, L. Atmani, E. H., Comparative study for highly Al and Mg doped ZnO thin films elaborated by sol gel method for photovoltaic application, **Journal of Applied Physics**, 121, 135103, (2017).

[16] Chauhan, J., Shrivastav, N., Dugaya, A., Pandey, D., Synthesis and Characterization of Ni and Cu Doped ZnO. **Journal of Nanomed Nanotechnol**., 8, (2017).

[17] Liu, Y., Yang, J., Guan, Q., Yang, L., Zhang, Y., Wang, Y., Feng, B., Cao, J., Liu, X., Yang, Y., Wei, M., Effects of Cr-doping on the optical and magnetic properties in ZnO nanoparticles prepared by sol–gel method, **Journal of Alloys and Compounds**, 486. 835–838, (2009).

[18] Kuo, S., Chen, W., Lai, F., Cheng, C., Kuo, S., Wang, H., Hsieh, W., Effects of doping concentration and annealing temperature on properties of highly-oriented Al-doped ZnO films, **Journal of Crystal Growth**, 287, 78–84, (2006).

[19] Akdağ, A., Budak, H. F., Yılmaz, M., Efe, A., Büyükaydın, M., Can, M., Turgut, G., Sönmez, E., Structural and Morphological Properties of Al doped ZnO Nanoparticles, **Journal of Physics: Conference Series**, 707, 012020, (2016).

[20] Zhou, H., Yi, D., Yu, Z., Xiao, L., Li, J., Preparation of aluminum doped zinc oxide films and the study of their microstructure, electrical and optical properties, **Thin Solid Films**, 515, 6909–6914, (2007).

[21] Garces, F. A., Budini, N., Koropecki, R. R., Arce, R. D., Structural Analysis of ZnO(:Al,Mg) Thin Films by X-ray Diffraction, **Procedia Materials Science**, 8, 551 –560, (2015).

[22] Chitraa, M., Uthayarani, K., Rajasekaran, N., Girijac, E. K., Preparation and characterisation of Al doped ZnO nanopowders, **Physics Procedia**, 49, 177–182, (2013).

[23] Köseoğlu, Y., Rapid synthesis of room temperature ferromagnetic Fe and Co co-doped ZnO DMS nanoparticles, **Ceramics International**, 41, 11655–11661, (2015).

[24] Ghosh, A., Kumari, N., Bhattacharjee, A., Influence of Cu doping on the structural, electrical and optical properties of ZnO, **Pramana journal of physics**, 84, 621–635, (2015).

[25] Osali, S., Esfahani, H., Karami, H., Effect of Al doping on crystallography and electro-optical properties of ZnO semiconductor thin films prepared by electrospinning, **Solid State Sciences**, 83, 90–98, (2018).

[26] Suwanboon, S., Amornpitoksuk, P., Preparation of Mg-doped ZnO nanoparticles by mechanical milling and their optical properties, **Procedia Engineering**, 32, 821–826, (2012).

[27] Beltran, J. J., Osorio, J. A. , Barrero, C. A., Hanna, C. B., Punnoose, A., Magnetic properties of Fe doped, Co doped, and Fe+Co co-doped ZnO, **Journal of Applied Physics**, 113, 17C308, (2013).

[28] Mote, V. D., Dargad, J. S., Dole, B. N., Effect of Mn Doping Concentration on Structural, Morphological and Optical Studies of ZnO Nano-particles. **Nanoscience and Nanoengineering**, 1, 116-122, (2013).

[29] Seetawan, U., Jugsujinda, S., Seetawan, T., Ratchasin, A., Euvananont, C., Junin, C., Thanachayanont, C., Chainaronk, P., Effect of Calcinations Temperature on Crystallography and Nanoparticles in ZnO Disk, **Materials Sciences and Applications**, 2, 1302-1306, (2011).

[30] Özgür, Ü., Alivov, Ya. I., Liu, C., Teke, A., Reshchikov, M. A., Doğan, S., Avrutin,V., Cho, S.-J., Morkoç, H., A comprehensive review of ZnO materials and devices, **Journal of Applied Physics**, 98, 041301, (2005).

[31] Baghdad, R., Lemee, N., Lamura, G., Zeinert, A., Hadj-Zoubir, N., Bousmaha, M., Bezzerrouk, H. Bouyanfif, M. A., Allouche, B., Zellama, K., Structural and magnetic properties of Co-doped ZnO thin films grown by ultrasonic spray pyrolysis method, **Superlattices and Microstructures**, 104, 553-569, (2017).

[32] Pradeev raj, K., Sadaiyandi, K., Kennedy, A., Sagadevan, S., Chowdhury, Z. Z., Johan, M. R. B., Aziz, F. A., Rafique, R. F., Selvi, R. T., Bala, R. R., Influence of Mg Doping on ZnO, Nanoparticles for Enhanced Photocatalytic Evaluation and Antibacterial Analysis, **Nanoscale Research Letters**, 13, 229, (2018).

[33] Fajar, A., Kartini, G. E., Mugirahardjo, H., Ihsan, M., Crystallite Size and Microstrain Measurement of Cathode Material after Mechanical Milling using Neutron Diffraction Technique, **Atom Indonesia**, 36, 111-115, (2010).

[34] Kumar, B. R., Hymavathi, B., X-ray peak profile analysis of solid-state sintered alumina doped zinc oxide ceramics by Williamson–Hall and size-strain plot methods, **Journal of Asian Ceramic Societies**, 5, 94–103, (2017).

[35] Saravanan, S., Silambarasan, M., Soga, T., Structural, morphological and optical studies of Ag-doped ZnO nanoparticles synthesized by simple solution combustion method, **Japanese Journal of Applied Physics**, 53, 11RF01, (2014).

[36] Yakuphanoglu, F., Electrical characterization and device characterization of ZnO microring shaped films by sol–gel method, **Journal of Alloys and Compounds**, 507, 184–189, (2010).

[37] Aydın, C., Abd El, M. S., Zheng, K., Yahia, I. S., Yakuphanoglu, F., Synthesis, diffused reflectance and electrical properties of nanocrystalline Fe-doped ZnO via sol–gel calcination technique, **Optics & Laser Technology**, 48, 447–452, (2013).

[38] Caglar, M., Ilican, S., Caglar, Y., Yakuphanoglu, F., Electrical conductivity and optical properties of ZnO nanostructured thin film, **Applied Surface Science**, 255, 4491–4496, (2009).

[39] Suwanboon, S., Amornpitoksuk, P., Sukolrat, A., Dependence of optical properties on doping metal, crystallite size and defect concentration ofbM-doped ZnO nanopowders (M= Al, Mg, Ti), **Ceramics International**, 37, 1359–1365, (2011).

[40] Suwanboon, S., Amornpitoksuk, P., Bangrak, P., Synthesis, characterization and optical properties of Zn1-xTixO nanoparticles prepared via a high-energy ball milling technique, **Ceramics International**, 37, 333–340, (2011).

[41] Xiong, G., Pal, U., Serrano, J. G., Ucer, K. B., Williams, R. T., Photoluminescence and FTIR study of ZnO nanoparticles: the impurity and defect perspective, **Physica status solidi (c),** 3, 3577–3581, (2006).

[42] Singhal, S., Kaur, J., Namgyal, T., Sharma, R., Cu-doped ZnO nanoparticles: Synthesis, structural and electrical properties, **Physica B**, 407, 1223–1226, (2012).

[43] Mallika, A. N., Reddy, A. R., Babu, K., Sujatha, C., Reddy, K. V., Structural and photoluminescence properties of Mg substituted ZnO Nanoparticles, **Optical Materials**, 36, 879–884, (2014).

[44] Elilarassi, R., Chandrasekaran, G., Microstructural and photoluminescence properties of Co-doped ZnO films fabricated using a simple solution growth method, **Materials Science in Semiconductor Processing**, 14, 179–183, (2011).